PERGAMON

Scripta Materialia 46 (2002) 401–406

www.actamat-journals.com

Linking phase-field model to CALPHAD: application to precipitate shape evolution in Ni-base alloys

J.Z. Zhu *, Z.K. Liu, V. Vaithyanathan, L.Q. Chen

Department of Materials Science and Engineering, The Pennsylvania State University, 119 Steidle Building, University Park, PA 16802-5005, USA

Received 9 October 2001; accepted 5 December 2001

Abstract

A three-dimensional phase-field model is proposed with the thermodynamic and kinetic parameters directly extracted from existing databases using the CALPHAD method. We modelled the γ' precipitate microstructure evolution in a Ni-base alloy, particularly a single precipitate morphology at different sizes using independently assessed thermodynamic, kinetic and structural parameters. © 2002 Published by Elsevier Science Ltd. on behalf of Acta Materialia Inc.

Keywords: Phase field; CALPHAD; Ni-base alloys; Microstructure; Computer simulation

1. Introduction

The phase-field approach has found increasing applications in modelling phase transformation and microstructural evolution in solids [1]. One of its main advantages is that the temporal evolution of any arbitrary microstructures can be predicted without any a priori assumptions about their evolution path. For example, it has been used to explain many of the morphological evolutions in coherent solids including Ni-base superalloys [2–5].

Despite the tremendous success of phase-field modelling in predicting many of the experimentally observed microstructures in solids, additional progress is required in order to apply it to predict the microstructure evolution in real multi-component alloy systems. For example, there exists no systematic approach for obtaining the thermodynamic and kinetic input to the phase-field models although a number of efforts have been reported in connecting phase-field models with existing thermodynamic and kinetic databases. Furthermore, the dependence of kinetic parameters such as diffusional mobility of atoms and of mechanical properties such as elastic constants on the composition is generally ignored whereas in real systems they are almost always composition dependent. Finally, existing phase-field simulations have been largely confined to two-dimension and the extension to three-dimensional (3D) systems requires efficient numerical algorithms.

The main purpose of this paper is to describe our initial attempt to develop a 3D phase-field model for modelling the microstructure evolution in Ni-base superalloys. The local free energy as a function

* Corresponding author. Tel.: +1-814-8650389; fax: +1-814-8670476.

E-mail address: zhu@cerse.psu.edu (J.Z. Zhu).

1359-6462/02/$ - see front matter © 2002 Published by Elsevier Science Ltd. on behalf of Acta Materialia Inc.
PII: S1359-6462(02)00013-1

of composition and order parameters is directly constructed using the CALPHAD method. Efficient iterative method and semi-implicit spectral methods are developed for solving the inhomogeneous elastic equilibrium equation and the field equations which take into account the composition dependence of atomic mobilities. In particular, we examine the morphological evolutions of a single precipitate as well as of a multi-precipitate system at a typical service temperature of 1300 K.

2. Model description

The phase-field model describes a microstructure by using a set of field variables. In Ni-base alloys, the $(\gamma' + \gamma)$ two-phase microstructure can be described by a composition field variable $c(\mathbf{r})$, and a three-component long-range order parameter field $\eta_i(\mathbf{r})$ $(i = 1, 2, 3)$. The composition field describes the local compositional distribution of all the species in a microstructure, whereas the long-range order parameter field describes the four types of possible $L1_2$ ordered domains related by a lattice translation and distinguishes the structural difference between ordered precipitates and the disordered matrix related by the $L1_2$ ordering.

Within the phase-field description, the total free energy of a microstructure, including the local chemical free energy, elastic energy and interfacial energy, can be written as a function of all field variables. The precipitation of γ' phase is driven by the local free energy difference between the disordered fcc γ phase and the equilibrium two-phase mixture of the ordered γ' particles contained in the disordered γ matrix. In most of the existing phase-field descriptions of the local chemical free energy, a Landau-type polynomial form is constructed as only an approximation [2–5]. Most parameters in the polynomials, which have no physical meanings, have to be determined empirically with trial and error. In this paper we show that the local chemical free energy can be directly constructed using the CALPHAD method [6,7] and thus relies on existing thermodynamic databases to supply the necessary thermodynamic input.

In the CALPHAD method, the Gibbs energy of individual phases is modelled from their crystallography information, and the model parameters are optimized through coupling of phase equilibrium and thermochemical data obtained from experimental measurements and first-principles calculations. To consider the disordered and ordered fcc phases in the Ni–Al system using a single Gibbs energy function of composition and temperature, a four-sublattice model is used with Ni and Al soluble in each sublattice [8]. The mole fraction of Ni and Al in each sublattice can then be represented by the three-component order parameter η_i. The Gibbs energy of the two-phase system including both ordered and disordered structures can be written in terms of the composition and the order parameter field as,

$$g(c,\eta_1,\eta_2,\eta_3) = g^{\mathrm{dis}}(c) + g^{\mathrm{order}}(c,\eta_1,\eta_2,\eta_3) - g^{\mathrm{order}}(c,\eta_i = 0) \tag{1}$$

g^{dis} and g^{order} are the Gibbs free energies of the disordered phase and ordered phase respectively which can be given by

$$\begin{aligned} g^{\mathrm{dis}} &= g_0^{\mathrm{dis}} + \Delta g_{\mathrm{ideal}}^{\mathrm{dis}} + \Delta g_{\mathrm{xs}}^{\mathrm{dis}} + \Delta g_{\mathrm{mag}}^{\mathrm{dis}} \\ g^{\mathrm{order}} &= g_0^{\mathrm{order}} + \Delta g_{\mathrm{ideal}}^{\mathrm{order}} + \Delta g_{\mathrm{xs}}^{\mathrm{order}} \end{aligned} \tag{2}$$

where

$$\begin{aligned} g_0^{\mathrm{dis}} &= c g_0^{\mathrm{Al}} + (1-c) g_0^{\mathrm{Ni}} \\ \Delta g_{\mathrm{ideal}}^{\mathrm{dis}} &= RT[c\ln(c) + (1-c)\ln(1-c)] \\ \Delta g_{\mathrm{xs}}^{\mathrm{dis}} &= c(1-c)[L_0 + L_1(2c-1) + L_2(2c-1)^2 \\ &\quad + L_3(2c-1)^3] \\ \Delta g_{\mathrm{mag}}^{\mathrm{dis}} &= RT\ln(\beta+1) f(\tau) \\ g_0^{\mathrm{order}} &= 6U_1 c^2 \sum \eta_i^2 \\ \Delta g_{\mathrm{ideal}}^{\mathrm{order}} &= \\ &\quad (RT/4)\{[c(1+\eta_1+\eta_2+\eta_3)]\ln[c(1+\eta_1+\eta_2+\eta_3)] \\ &\quad + [1-c(1+\eta_1+\eta_2+\eta_3)]\ln[1-c(1+\eta_1+\eta_2+\eta_3)] \\ &\quad + [c(1-\eta_1-\eta_2+\eta_3)]\ln[c(1-\eta_1-\eta_2+\eta_3)] \\ &\quad + [1-c(1-\eta_1-\eta_2+\eta_3)]\ln[1-c(1-\eta_1-\eta_2+\eta_3)] \\ &\quad + [c(1-\eta_1+\eta_2-\eta_3)]\ln[c(1-\eta_1+\eta_2-\eta_3)] \\ &\quad + [1-c(1-\eta_1+\eta_2-\eta_3)]\ln[1-c(1-\eta_1+\eta_2-\eta_3)] \\ &\quad + [c(1+\eta_1-\eta_2-\eta_3)]\ln[c(1+\eta_1-\eta_2-\eta_3)] \\ &\quad + [1-c(1+\eta_1-\eta_2-\eta_3)]\ln[1-c(1+\eta_1-\eta_2-\eta_3)]\} \\ \Delta g_{\mathrm{xs}}^{\mathrm{order}} &= -2U_1 c^2 \sum \eta_i^2 + 12U_4(1-2c)c^2 \\ &\quad \times \sum \eta_i^2 - 48U_4 c^3 \eta_1\eta_2\eta_3 \end{aligned} \tag{3}$$

All the parameters and functions in Eq. (3) such as g_0^{Al}, g_0^{Ni}, L_0, L_1, L_2, L_3, β, $f(\tau)$, U_1, and U_4 can be obtained from CALPHAD database as a function of temperature [8].

At a constant temperature and composition, the local free energy as a function of composition for the precipitate phase can be determined by minimizing the free energy with respect to the order parameters, i.e. $g(c, \eta_{i0}(c))$. The corresponding local free energy for the disordered matrix phase can be obtained by setting all the three components of the order parameter to zero, i.e. $g(c, \eta_i = 0)$. From the two free energy curves as a function of composition, the equilibrium compositions of the two-phase mixtures at a given temperature can be obtained by constructing a common tangent. Fig. 1 plots the chemical free energy as a function of composition at 1300 K where one curve describes the disordered γ phase and another describes the ordered γ' phase. The equilibrium composition values of the two phases at the stress-free state at 1300 K are determined to be 0.165 and 0.230, respectively. The maximum driving force Δg_{max} at 1300 K is approximately 125 J/mol as seen from Fig. 1.

In the diffuse-interface phase-field model, the interfacial energy between the precipitate and the matrix is introduced through the gradients of the field variables. Denote $f(c, \eta_i)$ as the Helmholtz free energy density converted from the Gibbs free energy density $g(c, \eta_i)$. A general form for the total stress-free chemical free energy can be written as [9]

$$F_c = \int_V \left[f(c, \eta_i) + \frac{\alpha}{2}(\nabla c)^2 + \sum_{p=1}^{3} \frac{\beta_{ij}(p)}{2} \nabla_i \eta_p \nabla_j \eta_p \right] \mathrm{d}V \tag{4}$$

where $\nabla_i = \partial/\partial x_i$ is the ith component of the vector operator ∇ and x_i is the ith component of the spatial coordinate vector $\mathbf{r}$. In Eq. (4), α and $\beta_{ij}(p)$ are gradient energy coefficients, which control the diffuse-interface thickness, need to be determined from the experimentally measured interfacial energy and anti-phase boundary (APB) energy. The gradient energy coefficient for the orientation field variables $\beta_{ij}(p)$ is written in a tensor form so as to incorporate the interfacial energy anisotropy. For simplicity isotropic interfacial energy is assumed in this paper. The elastic strain energy has an important contribution to the total free energy. We have developed an efficient iterative method for solving an elastically anisotropic coherent system with elastic inhomogeneity to compute the elastic energy E_{el} [10]. The total free energy F is the sum of the incoherent free energy F_c and the coherent elastic energy E_{el}, i.e. $F = F_c + E_{el}$. The temporal evolution of field variables is described by time-dependent kinetic field equations—namely, the Cahn–Hilliard equations for the composition field and the Ginzburg–Laudau equations for the long-range order parameters fields. The morphological evolution during the precipitation and coarsening can be obtained by solving the four non-linear kinetic [11,12]:

$$\frac{\partial c(\mathbf{r}, t)}{\partial t} = \nabla \cdot \left[M(\mathbf{r}, t) \nabla \frac{\delta F}{\delta c(\mathbf{r}, t)} \right] + \xi(\mathbf{r}, t) \tag{5}$$

$$\frac{\partial \eta_i(\mathbf{r}, t)}{\partial t} = -K \frac{\delta F}{\delta \eta_i(\mathbf{r}, t)} + \zeta_i(\mathbf{r}, t) \tag{6}$$

where $i = 1, 2, 3$. c is the composition of Al. K and M are kinetic coefficients for the two field

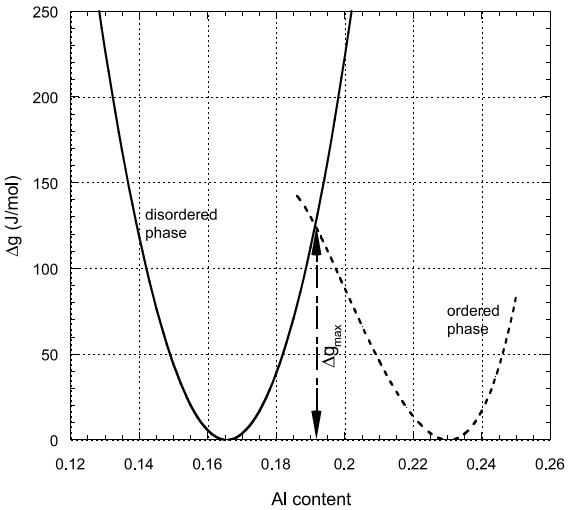

Fig. 1. Calculated chemical free energy as a function of composition for both the disordered and ordered phase at 1300 K.

variables. $M(\mathbf{r},t)$ describes a composition-dependent mobility which can be written as $M = c(1-c)[cM_{\mathrm{Ni}} + (1-c)M_{\mathrm{Al}}]$. M_{Ni} and M_{Al} are the atomic mobilities of Ni and Al which can be calculated from kinetic database at a given temperature [13]. $\xi(\mathbf{r},t)$ and $\zeta_i(\mathbf{r},t)$ are noise terms which generate fluctuations in the composition and structural order parameter fields. We employ an accurate and efficient semi-implicit Fourier spectral method for solving the two kinetic equations [14].

3. Results and discussion

Our simulations are performed on a cubic domain with periodic boundary conditions. The gradient coefficients α and β_{ij} are determined from measured γ' matrix interfacial free energy and the APB energy on $\{1\,0\,0\}$. To avoid some huge or very small numbers involved in the computation, the parameters are scaled by reduced time $t^* = Kt\Delta g_{\max}$ and $r^* = r/l$ where l represents the length scale of the system [4]. The typical input parameters used for the two field equations at 1300 K are unit grid size $\Delta x = 1$ nm, scaled time step $\Delta t^* = 0.02$, compositional gradient coefficient $\alpha = 2.524 \times 10^{-9}$ J/m, order parameter gradient coefficients $\beta_{ij} = 7.29 \times 10^{-12}$ J/m, scaled average mobility $\bar{M}^* = \bar{M}/(Kl^2) = 0.007937$, and the lattice mismatch $\delta = 0.00294$ [15]. The elastic constants of the two phases are estimated from Refs. [16,17] as $C_{11}^{\gamma} = 195.8$ GPa, $C_{12}^{\gamma} = 144.0$ GPa, $C_{44}^{\gamma} = 89.6$ GPa, $C_{11}^{\gamma'} = 194.64$ GPa, $C_{12}^{\gamma'} = 141.8$ GPa, and $C_{44}^{\gamma'} = 91.9$ GPa.

To investigate the shape evolution of the γ' precipitate, we first studied a single particle evolution where the interaction among precipitates is ignored. Under an aging temperature of 1300 K, a spherical γ' particle with the equilibrium composition $c_{\gamma'} = 0.230$ and order parameter values $\eta_i = 0.948288$ was initially embedded in the γ matrix ($c_{\gamma} = 0.165$, $\eta_i = 0$). The shape evolution of the particle will then be mainly determined by the balance between the interfacial energy and elastic energy relaxation, which are included in the variational derivatives in the kinetic equations (5) and (6). Fig. 2(a) shows the shape evolution of a single particle with a radius of 16 nm in a $48 \times 48 \times 48$ lattice at three different times. It can be seen that the particle remains a near-spherical shape at its length scale (~30 nm in Fig. 2(a)). When the particle is small in size, the interfacial energy will dominate in the total energy and thus equilibrium particle shape will be that of a minimal interfacial energy, which is spherical due to the isotropic interfacial energy.

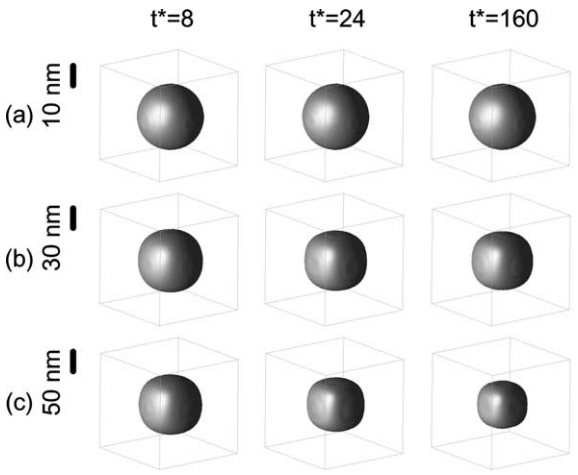

Fig. 2. Shape evolution of a single γ' particle at different length scales.

An increase in particle size requires more number of points used for the particle in a discretized lattice. To remain a constant particle volume percentage where the boundary effects can be neglected, a larger system size is therefore needed for a larger particle size. However, an increase of the system size will increase the computational time and memory dramatically, especially when a 3D system is considered. To simulate the effects of particle size on the equilibrium shape without having to run simulations in a large system size, we introduce a dimensionless parameter size L to characterize the ratio of the elastic energy to the interfacial energy [18,19]. Assuming $\bar{l}$ as the average length scale of the particle, $\bar{\lambda}$ as the effective elastic constant to characterize the average stiffness, $\bar{\varepsilon}$ as the average elastic strain, γ_{s} as the surface energy density, L is defined by

$$L = \frac{\bar{\lambda}\bar{\varepsilon}^2\bar{l}^3}{\gamma_{\mathrm{s}}\bar{l}^2} = \frac{\bar{l}}{l_0} \tag{7}$$

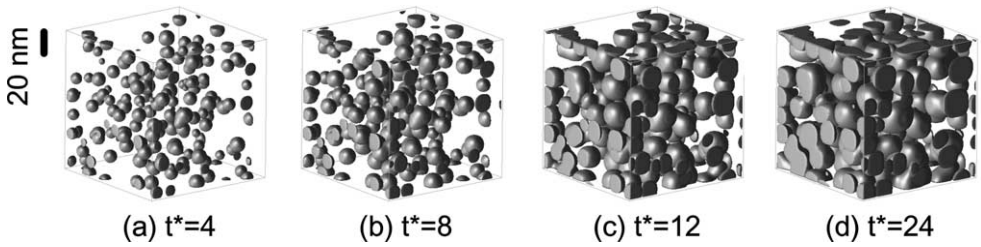

Fig. 3. Morphological evolution from 3D simulations showing the nucleation, growth and coarsening of γ' precipitates at 1300 K.

where $l_0 = \gamma_s/(\bar{\lambda}\bar{\varepsilon}^2)$ can be regarded as a kind of material constant that has a dimension of an length ($\sim$10 nm for Ni–Al at 1300 K). The real average length scale $\bar{l}$ will be proportional to the dimensionless parameter L, and therefore, different real length scale can be reached by different L values. The parameter L can be changed by the ratio of total elastic energy to the interfacial energy. For example, double elastic energy E_{el} will double L, which will achieve very similar effect of double the average length scale $\bar{l}$. Fig. 2(b) and (c) illustrate the morphologies of the γ' particle evolving as a function of time where $L = 3$ and $L = 5$ respectively with their corresponding real length scales are shown. The particle gradually becomes cuboidal that is more or less cubic in shape with rounded edges and corners. It acquires slightly curved convex interfaces parallel to the elastic soft $\{100\}$ directions. As the interfacial energy is proportional to the interfacial area and the elastic energy is proportional to the particle volume, the elastic energy part of the total energy will dominate at large particle size, which drives the particle shape change from spherical to cuboidal in an elastically anisotropic system. In Fig. 2(b) and (c), the corresponding real particles sizes are approximately 80 nm (Fig. 2(b)) and 110 nm (Fig. 2(c)). As seen from Fig. 2, the equilibrium precipitate volume fraction decreases with increasing L. It decreases from 15% in Fig. 2(a) ($L = 1$) to 6% in Fig. 2(c) ($L = 5$), indicating the ratio of elastic energy to interfacial energy has important influence on the equilibrium compositions of the two phases. We find that the computed equilibrium compositions c_γ and $c_{\gamma'}$ of the two phases have changed from 0.167 and 0.230 for $L = 1$ to 0.173 and 0.222 for $L = 5$, resulting in the decrease of the equilibrium particle volume fraction.

To represent a real 3D Ni–Al system we need to investigate the multi-particle interaction effects which play an important role in determining the morphology of particles as well as their spatial arrangement. Fig. 3 shows an example of microstructural evolution in a lattice with $128 \times 128 \times 128$ grid points at an equilibrium particle volume fraction $\sim$35%. Initially the system is prepared in a high-temperature homogeneous initial state where the composition deviation from the average value is only caused by fluctuation. The nucleation, growth and coarsening of γ' particles are evident in Fig. 3, driven by the decrease of the total free energy. During the nucleation and growth periods where the particle size is small, the particles are spherical (Fig. 3(a) and (b)). The average domain size increases at later times accompanying with the particle shape changing to cuboidal. Particle coarsening by the coalescence of neighboring domains are observed.

For a single particle in Ni–Al alloy system aging at 1300 K, it can be predicted from Fig. 2 that the shape evolution from spherical to cuboidal occurs in the length scale of approximately 80 nm. However, in a multi-particle system with high volume fraction where the elastic interaction energies cannot be neglected, such a shape change occurs even at smaller particle size 15–20 nm as shown in Fig. 3(d). The predicted length scale is in good agreement with experimental observations [20]. With the length scale and thermodynamic and kinetic parameters considered in our work, we did not observe γ' developing to concave cuboidal

particles and plates or undergoing splitting to form doublets or octets, which should occur only when the particle size grows to a very large length scale.

In summary, we have developed a 3D phase-field model to link with CALPHAD method through the local free energy construction as a function of field variables where most important thermodynamic and kinetic parameters are taken from either a database or independent experimental measurements. The compositional dependence of atomic mobilities and elastic constants is taken into account in solving the phase-field equations and elastic equilibrium equations. The Ni_3Al precipitate shape evolution in a disordered fcc matrix, as illustrated from the simulations, depends on the balance between the interfacial energy and the elastic energy relaxation. Carrying out 3D simulations in a larger system size is currently underway to have a complete analysis of the precipitate coarsening behavior in Ni-base superalloys.

Acknowledgements

The authors are grateful for financial support from NASA under grant no. NCC3-920 and from the National Science Foundation under grant nos. DMR-0122638 and DMR-9983532. The simulation was performed at the San Diego Supercomputer Center.

References

[1] Chen LQ, Wang YZ. JOM 1996;48:13.
[2] Wang Y, Banerjee D, Su CC, Khachaturyan AG. Acta Mater 1998;46:2983.
[3] Li DY, Chen LQ. Scripta Mater 1997;37:1271.
[4] Rubin G, Khachaturyan AG. Acta Mater 1999;47:1995.
[5] Vaithyanathan V, Chen LQ. In: Nucleation and growth processes in materials. Massachusetts: MRS; 2000. p. 327.
[6] Kaufman L, Bernstein H. Computer calculation of phase diagrams with special reference to refractory metals. New York: Academic Press; 1970.
[7] Saunders N, Miodownik AP. CALPHAD (calculation of phase diagrams): a comprehensive guide. Oxford, New York: Pergamon; 1998.
[8] Ansara I, Dupin N, Lukas HL, Sundman B. J Alloy Compd 1997;247:20.
[9] Cahn JW, Hilliard JE. J Chem Phys 1958;28:258.
[10] Hu SY, Chen LQ. Acta Mater 2001;49:1879.
[11] Cahn JW. Acta Metall 1961;9:795.
[12] Allen SM, Cahn JW. Acta Metall 1979;27:1085.
[13] Engstrom A, Hoglund L, Agren J. Metall Mater Trans A 1994;25:1127.
[14] Zhu JZ, Chen LQ, Shen J, Tikare V. Phys Rev E 1999; 60:3564.
[15] Kamara AB, Ardell AJ, Wagner CNJ. Metall Mater Trans A 1996;27;2888.
[16] Prikhodko SV, Carnes JD, Isaak DG, Yang H, Ardell AJ. Metall Mater Trans A 1999;30:2403.
[17] Prikhodko SV, Carnes JD, Isaak DG, Ardell AJ. Scripta Mater 1998;38:67.
[18] Ardell AJ, Kim DM. In: Phase transformation and evolution in materials. Pennsylvania: TMS; 2000. p. 309.
[19] Mueller R, Gross D. Comput Mater Sci 1998;11:35.
[20] Maheshwari A, Ardell AJ. Scripta Metall Mater Sci 1992; 26:347.